

Research Article

Open Access



Crystalline phase-dependent cations migration in core-shell lanthanide-doped upconversion nanoparticles

Chang-Yun Qin[#], Jia-Hui Gao[#], Xian-Bin Xie, Chun-Peng Zhai, Hui-Qiao Li, Ying Ma^{*}

State Key Laboratory of Materials Processing and Die & Mould Technology, School of Materials Science and Engineering, Huazhong University of Science and Technology, Wuhan 430074, Hubei, China.

[#]These authors contribute equally

***Correspondence to:** Prof. Ying Ma, State Key Laboratory of Materials Processing and Die & Mould Technology, School of Materials Science and Engineering, Huazhong University of Science and Technology, Wuhan 430074, Hubei, China. E-mail: yingma@hust.edu.cn

How to cite this article: Qin CY, Gao JH, Xie XB, Zhai CP, Li HQ, Ma Y. Crystalline phase-dependent cations migration in core-shell lanthanide-doped upconversion nanoparticles. *Chem Synth* 2023;3:29. <https://dx.doi.org/10.20517/cs.2023.06>

Received: 19 Mar 2023 **First Decision:** 4 Apr 2023 **Revised:** 27 Apr 2023 **Accepted:** 30 May 2023 **Published:** 9 Jun 2023

Academic Editors: Bao-Lian Su, Da-Gang Yu **Copy Editor:** Dan Zhang **Production Editor:** Dan Zhang

Abstract

Core-shell structures are widely used to modulate upconversion emission or mitigate surface quenching and cross-relaxation in lanthanide-doped upconversion nanoparticles (UCNPs) to meet the requirements of various applications. Interfacial cation migration has been found recently to deteriorate the core-shell structures and thus affect their upconversion luminescence when they are subjected to annealing post-treatment. Herein, we demonstrate that the interfacial cation migration largely depends on the crystalline phase of the host lattice. Significant $\text{Er}^{3+}/\text{Y}^{3+}(\text{Yb}^{3+})$ diffusion and migration occur across the core-shell interface when cubic NaREF_4 ($\text{RE} = \text{Y}, \text{Yb}, \text{Er}$) core-shell or core-shell-shell UCNPs are annealed at 200 °C in the solid state, while the cation migration in hexagonal counterparts is negligible and the core-shell (core-shell-shell) structure can be well maintained in the same condition. The loosely packed atoms and large cubic void surrounded by eight F⁻ ions in cubic NaREF_4 lattice may facilitate cations diffusion and migration, enabling interfacial cations migration at relatively lower temperature. This finding may help us better understand temperature-dependent upconversion luminescent properties of core-shell UCNPs and better utilize various core-shell structured UCNPs according to different requirements of applications.

Keywords: Upconversion nanoparticles, core-shell interface, interfacial cation migration



© The Author(s) 2023. **Open Access** This article is licensed under a Creative Commons Attribution 4.0 International License (<https://creativecommons.org/licenses/by/4.0/>), which permits unrestricted use, sharing, adaptation, distribution and reproduction in any medium or format, for any purpose, even commercially, as long as you give appropriate credit to the original author(s) and the source, provide a link to the Creative Commons license, and indicate if changes were made.



INTRODUCTION

Different from downshifting emission often observed in conventional fluorophores and semiconductor quantum dots, lanthanide-doped upconversion nanoparticles (UCNPs) can emit high-energy photons via sequential absorption of two or multiple low-energy photons thanks to their abundant intermediate energy levels. In addition to their fascinating luminescent properties such as large anti-stoke shift, long lifetime, and sharp multiline emission ranging from UV to NIR, high chemical stability and low toxicity of lanthanide-doped UCNPs enable a broad range of applications, especially in background-free bio-sensing and biomedical domains^[1-9]. Nevertheless, wider applications from bench to clinical practice are still severely hindered by their limited upconversion efficiencies and brightness.

Numerous strategies have been developed to enhance the upconversion luminescence (UCL) of lanthanide-doped UCNPs over the past two decades^[10-16]. Among these, core-shell structures, represented by distinct distribution or separation of various lanthanide ions, have been widely adopted and demonstrated to be one of the most effective strategies for promoting energy transfer efficiency and modulating energy migration pathways^[17-20]. Since the peculiar or highly efficient UCL of these core-shell UCNPs is largely dependent on the distribution of lanthanide ions within them, their structure integrality and invariability are significantly important for maintaining their UCL. Besides cation diffusion and intermixing demonstrated in single- and multi-shell UCNPs during epitaxial growth of the shell, leading to a solid-solution-like interface^[21-23], cation migration and photoluminescent variation during the post-annealing process of core-shell UCNPs have recently attracted great attention. The diffusion and migration of Ce³⁺/Tb³⁺ across the core-shell interface were first validated after annealing of NaYF₄: Ce@NaYF₄: Tb core-shell nanoparticles in the solid state at temperatures higher than approximately 350 °C^[24]. Subsequently, Zhang *et al.* found that the elemental migration occurred more easily during the post-annealing progress in an OA/ODE solution, and the migration efficiency was influenced by the relative lanthanide ion radius^[25]. In our previous work, we demonstrated that the upconversion quantum yield of UCNPs could be significantly promoted in both cubic and hexagonal phase NaREF₄ (RE = Y, Yb, Er) nanoparticles through core-shell structure engineering, where Er³⁺ activators and Yb³⁺ sensitizers are spatially separated^[26]. However, the cubic and hexagonal core-shell-shell nanoparticles exhibit a discrepancy in temperature-dependent photoluminescence. Therefore, it is necessary to investigate the diffusion and migration of lanthanide ions across the neighboring layers in the two crystal phases for better utilization of these core-shell UCNPs.

In this work, we synthesize cubic and hexagonal phase single- and double-shell NaREF₄ UCNPs via an epitaxial growth route and compare the cation migration across the interface of the neighboring layers in these two crystal phases. UCL performance and surface compositions of these UCNPs are collected before and after post-annealing to monitor the cation migration in the solid state. Our investigation reveals that the lanthanide cations are more prone to migrate across the interface in cubic nanoparticles compared to those in hexagonal counterparts.

EXPERIMENTAL

Materials

RE₂O₃ (RE=Y, Er, Yb; 99.99%), oleic acid (OA; 90%), 1-octadecene (ODE; 90%), yttrium chloride hexahydrate (YCl₃·6H₂O; 99.9%), erbium chloride hexahydrate (ErCl₃·6H₂O; 99.9%), ytterbium chloride hexahydrate (YbCl₃·6H₂O; 99.9%), sodium hydroxide (NaOH, 99.9%), and ammonium fluoride (NH₄F, 98%) were purchased from Sigma-Aldrich. CF₃COONa (NaTFA, 98%) was purchased from Alfa Aesar.

Trifluoroacetic acid (99.5%) was purchased from Aladdin Inc. Ethanol, methanol, and cyclohexane were purchased from Sinopharm Chemical Reagent Co., China. All chemicals were used as received without any further purification.

Preparation of Lanthanide Trifluoroacetate (RETFA) Precursors

YTFA, ErTFA, and YbTFA (lanthanide trifluoroacetate (RETFA, RE=Y, Er, Yb)) were prepared by a literature method^[27-28] with a slight modification. 50 mmol of RE₂O₃ was added in 50 mL trifluoroacetic acid aqueous solution. Then the mixture was heated to 95 °C under vigorous magnetic stirring until it became a transparent solution. The superfluous trifluoroacetic acid was evaporated, and the resultant solid RETFA was dissolved in 100 mL deionized water to prepare RETFA aqueous solution (1 M). 100 mmol of NaTFA was dissolved in 100 mL deionized water to acquire a stock solution (1 M).

Synthesis of α -NaYF₄:10%Er and α -NaErF₄ core nanoparticles

The cubic phase core nanoparticles were synthesized by the method we reported previously^[26]. First, 1 mmol of NaTFA and RETFA solutions was mixed with 5 mL OA, 5 mL OM, and 10 mL ODE in a 50 mL three-necked flask. Next, the mixture was heated to 120 °C for 30 min with continuous magnetic stirring under an Ar atmosphere to remove water and oxygen. Then the transparent solution was quickly heated to 300 °C for 1 h before cooling to room temperature. After excessive ethanol was added to the solution, the resultant mixture was centrifuged at 10000 rpm for 10 min, collected and re-washed with a cyclohexane/ethanol mixed solution several times, and dispersed in 10 mL cyclohexane.

Synthesis of α -NaYF₄:10%Er@NaYbF₄ and α -NaErF₄@NaYF₄ nanoparticles

The α -core-shell nanoparticles were synthesized by an epitaxial growth protocol taking the core nanoparticles as seeds. In a typical procedure to synthesize NaErF₄@NaYF₄ nanoparticles, 3 mL of NaTFA solution, 3 mL of YTFA solution, and 3 mL of core nanoparticle dispersion were mixed with 10 mL OA and 10 mL ODE in a 50 mL three-necked flask. The mixture was first heated to 90 °C for 30 min with continuous magnetic stirring under an Ar atmosphere to remove cyclohexane. Next, it was heated to 120 °C and kept for 30 min to evaporate water and oxygen. Subsequently, it was heated to 290 °C and kept for 30 min for epitaxial growth before cooling to room temperature. Finally, the resultant mixture was washed with cyclohexane/ethanol by a similar procedure to that utilized for washing the core nanoparticles.

Synthesis of α -NaYF₄:10%Er@NaYbF₄@NaYF₄ nanoparticles

The procedure for synthesizing double-shell nanoparticles was identical to that for synthesizing single-shell ones, except for using single-shell UCNPs as the seeds and different RETFA precursors.

Synthesis of β -NaYF₄:10%Er and β -NaErF₄ core nanoparticles

The hexagonal phase core nanoparticles were synthesized via a protocol reported by Wang *et al.*^[29] with a slight modification. In a typical procedure, 1 mmol of RECl₃·6H₂O was added into 6 mL OA and 15 mL ODE. Then the mixture was heated to 130 °C and kept for 30 min with continuous magnetic stirring under an Ar atmosphere to remove water until a clear lanthanide-oleate complexes solution formed. Subsequently, the solution was cooled to room temperature, and 6 mmol of NH₄F (in 10 mL methanol) and 3 mmol of NaOH were added and stirred for 30 min. Afterward, the mixture was heated to 85 °C for 2 h to remove methanol, followed by being heated to 300 °C for an hour before cooling to room temperature. Finally, the resultant nanoparticles were washed with cyclohexane and ethanol via the same procedure as the cubic core nanoparticles.

Synthesis of β -core-shell nanoparticles

The synthesis procedure for β -single/double-shell nanoparticles was identical to that utilized for synthesizing β -NaREF₄ core nanoparticles, except for adding core or single-shell nanoparticles dispersed in cyclohexane along with methanol solution.

Annealing of UCNPs films

The as-synthesized nanoparticles cyclohexane dispersions (0.02 mmol mL⁻¹) were cast into homogeneous films on quartz plates [Supplementary Figure 1]. The UCNPs films were quickly heated up to the setting temperature (heating rate: 30 °C min⁻¹) for some time in a tubular furnace under a slow Ar flow (50 sccm) after degassing under a steady Ar flow (500 sccm) for half an hour (“sccm” is the abbreviation of “standard cubic centimeter per minute”). To avoid the combustion or carbonization of surface ligands, the films were firstly heated at 250 °C for 2 h to remove surface ligands before they were heated to 400 °C, according to the TG curve of UCNPs [Supplementary Figure 2].

Nanoparticles characterization

The phase and crystal structure of the samples were characterized by using a powder X-ray diffractometer (XRD, PANalytical X'pert PRO-DY2198). The size and shape of the samples were observed via a transmission electron microscope (TEM, Jeol JEM 2100F) operated at an acceleration voltage of 200 kV. X-ray photoelectron spectroscopy (XPS) data were obtained using an ESCALab250 electron spectrometer from Thermo Fisher Scientific Corporation with monochromatic 150 W Al K α radiation. The binding energies were referenced to the C1s line at 284.8 eV from adventitious carbon. The UCL properties were recorded on an Edinburgh FLS 980 spectrofluorometer in conjunction with a continuous-wave (CW) 980 nm diode laser. An Oxford Instrument Microstat HiRes2 was used to obtain the emission spectra within 298-498 K. UCL lifetimes were measured with the same spectrofluorometer equipped with an optical parametric oscillator (OPO) as the excitation source (197-2750 nm, 20 Hz repetition rate, and about 3 ns pulse width).

RESULTS AND DISCUSSION

As a proof-of-concept experiment, we take the NaYF₄:10%Er@NaYbF₄@NaYF₄ structured UCNPs as an example, which is demonstrated to render high upconversion efficiencies^[26]. α/β -NaYF₄:10%Er@NaYbF₄@NaYF₄ trilayered UCNPs were synthesized by using thermal decomposition and co-precipitation strategies, respectively. α/β -NaYF₄ nanoparticles, single-doped with Er³⁺ (10%), were first synthesized and then served as cores for successive epitaxial growth of NaYbF₄ shell (the first layer) and NaYF₄ shell (the second layer) via the layer-by-layer growth process, which has been widely adopted by numerous groups^[17-23]. As shown in Figure 1, the as-prepared core, single-shell, and double-shell nanoparticles exhibit highly uniform morphology and size for both the α and β phases. The average size of α -NaYF₄ nanoparticles is determined to be about 11.1 \pm 0.5 nm by analysis of over 100 particles from the TEM image [Figure 1A]. After epitaxial growth of approximately 8.5 nm NaYbF₄ shell on the core nanoparticles, the as-synthesized α -NaYF₄:10%Er@NaYbF₄ core-shell nanoparticles are well dispersed with a sharp size distribution of 28.3 \pm 1.0 nm [Figure 1B]. Subsequently, a final inert NaYF₄ (about 2 nm thickness) is grown to suppress surface quenching, producing α -NaYF₄:10%Er@NaYbF₄@NaYF₄ nanoparticles with 32.9 \pm 1.0 nm [Figure 1C]. The average sizes of β -phase core (11.8 \pm 0.5 nm), core-shell (28.1 \pm 0.7 nm), and core-shell-shell UCNPs (32.5 \pm 0.8 nm) are also precisely controlled to be nearly the same as those α -counterparts [Figure 1D-F]. The X-ray diffraction (XRD) patterns of these multilayered UCNPs can be well-indexed to cubic (JCPDS file number 77-2042) and hexagonal (JCPDS file number 16-0334) phases of NaYF₄, respectively [Supplementary Figure 3A and B].

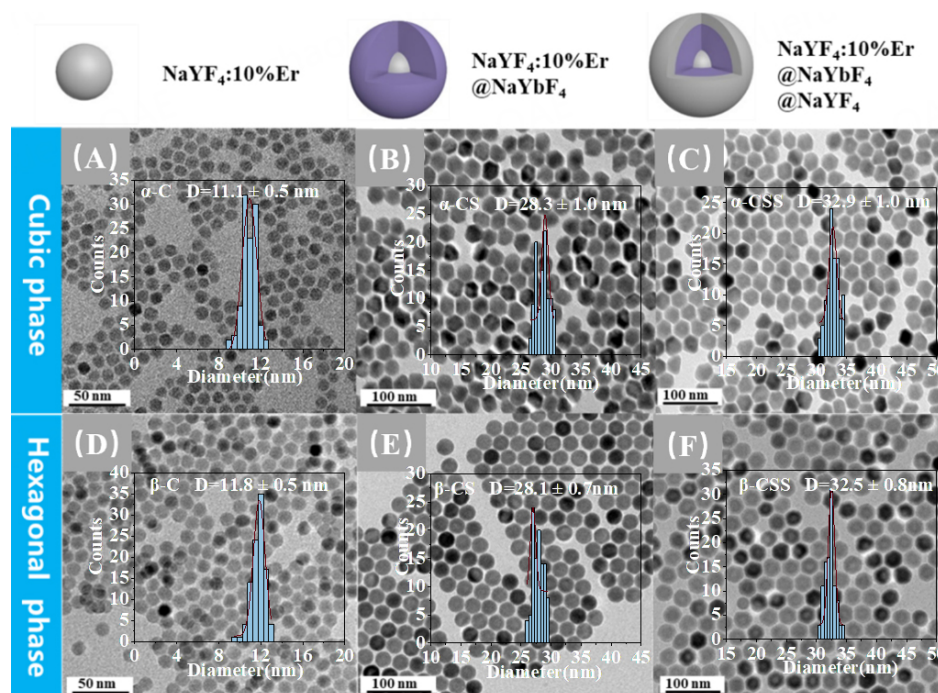


Figure 1. TEM images of cubic (A-C, α -phase) and hexagonal (D-F, β -phase) $\text{NaYF}_4\text{:10\%Er}$ core, $\text{NaYF}_4\text{:10\%Er @NaYbF}_4$ core-shell; $\text{NaYF}_4\text{:10\%Er@NaYbF}_4\text{@NaYF}_4$ core-shell-shell nanoparticles. The size distribution is shown in the insets.

These nanoparticles were then cast into homogeneous films on a quartz plate, and temperature-dependent UCL spectra of $\alpha/\beta\text{-NaYF}_4\text{:10\%Er@NaYbF}_4\text{@NaYF}_4$ UCNP films ranging from 298 to 498 K were collected, as shown in Figure 2. The upconversion emissions at 407, 540, and 651 nm of $\alpha/\beta\text{-NaYF}_4\text{:10\%Er@NaYbF}_4\text{@NaYF}_4$ UCNP films correspond to $^2\text{H}_{9/2} \rightarrow ^4\text{I}_{15/2}$, $^4\text{S}_{3/2} \rightarrow ^4\text{I}_{15/2}$, and $^4\text{F}_{9/2} \rightarrow ^4\text{I}_{15/2}$ transitions of Er^{3+} , respectively. Different from the inert core-active shell nanoparticles^[30], when the temperature increased, these upconversion emissions continuously decreased for either α or β -phase trilayered UCNP films as a result of the increasing multiphonon non-radiative relaxations^[26,31–32]. Once the films were cooled to room temperature, $\beta\text{-NaYF}_4\text{:10\%Er@NaYbF}_4\text{@NaYF}_4$ UCNP films recovered their emissions intensity [Figure 2B], while the intensity of upconversion emission at 407, 540, and 651 nm of $\alpha\text{-NaYF}_4\text{:10\%Er@NaYbF}_4\text{@NaYF}_4$ UCNP films dropped off about 45%, 39%, and 40%, respectively [Figure 2A]. This great discrepancy indicates structural integrity remains for β -phase UCNP films, and structural variation may have occurred for α -phase UCNP films during the heating process. To further amplify such discrepancy, we annealed $\alpha/\beta\text{-NaYF}_4\text{:10\%Er@NaYbF}_4\text{@NaYF}_4$ UCNP films at 200 °C for 4 h in a tubular furnace under a slow Ar flow.

XRD peaks of $\alpha/\beta\text{-NaYF}_4\text{:10\%Er@NaYbF}_4\text{@NaYF}_4$ UCNP films remained unchanged [Supplementary Figure 3A and B] after annealing at 200 °C for 4 h, suggesting that the particle size and crystalline phase were well preserved. Thus recrystallization and growth of the crystalline grains can be excluded, consistent with the morphology and phase maintaining of $\text{NaYF}_4\text{:Ce@NaYF}_4\text{:Tb}$ nanoparticles even after annealing at 350 °C^[24]. As expected, the upconversion emissions of Er^{3+} at 407, 540, and 651 nm are significantly decreased by about 70%, 65%, and 63% for $\alpha\text{-NaYF}_4\text{:10\%Er@NaYbF}_4\text{@NaYF}_4$ [Supplementary Figure 4], and the corresponding lifetimes changed from 0.42, 0.50, and 0.58 ms to 0.25, 0.28, and 0.36 ms, respectively [Figure 3]. Different from phase, the UCL and their corresponding decay times for $\beta\text{-NaYF}_4\text{:10\%Er@NaYbF}_4\text{@NaYF}_4$ UCNP films are well-maintained even after annealing for 4 h [Supplementary 5, Figure 4], suggesting the better structural integrity and invariability of β -core-shell-shell UCNP films compared with α -phase. Considering the size and crystalline phase of α -trilayered UCNP films hardly changed after annealing, $\text{Yb}^{3+}/\text{Er}^{3+}$

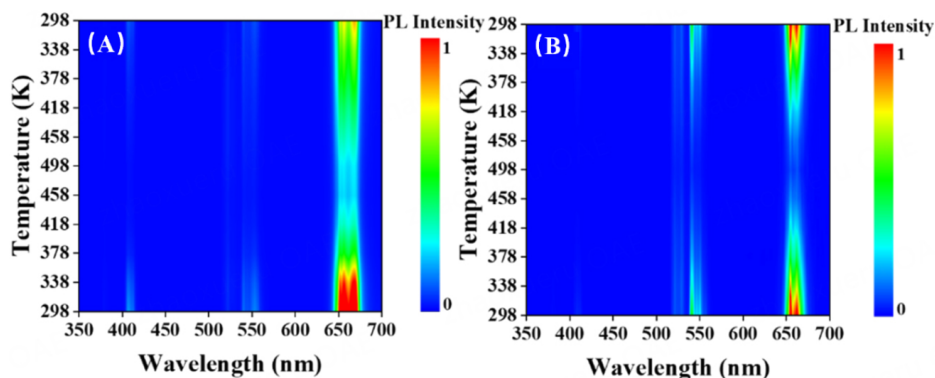


Figure 2. In-situ temperature-dependent UCL spectrum of α - (A) and β - (B) $\text{NaYF}_4\text{:10\%Er@NaYbF}_4\text{@NaYF}_4$ UCNPs under 980-nm excitation.

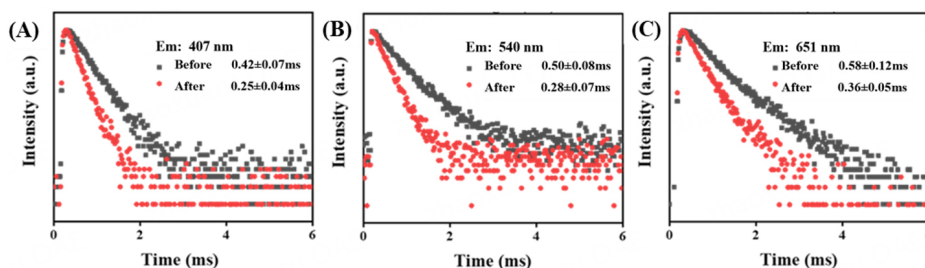


Figure 3. Decay curves at 407 (A); 540 (B); and 651 nm (C) for α - $\text{NaYF}_4\text{:10\%Er@NaYbF}_4\text{@NaYF}_4$ UCNPs before and after annealing at 200 °C for 4 h.

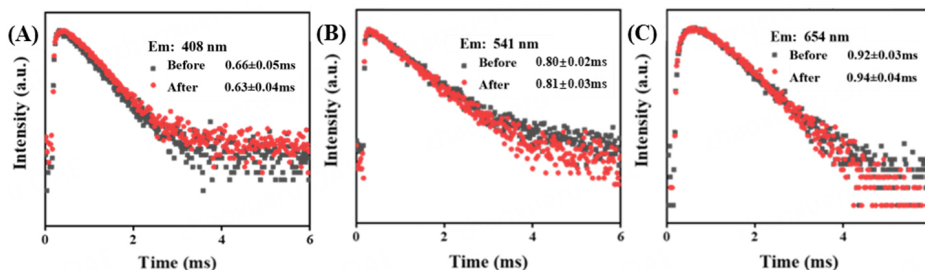


Figure 4. Decay curves at 408 (A); 541 (B); and 654 nm (C) for β - $\text{NaYF}_4\text{:10\%Er@NaYbF}_4\text{@NaYF}_4$ UCNPs before and after annealing at 200 °C for 4 h.

migration across the core-shell and shell-shell interface may be responsible for the significant decrease of UC emission intensity and the corresponding lifetime since the surface quenching will occur in this case.

Because $\text{Ce}^{3+}/\text{Tb}^{3+}$ migration across the core-shell interface could be detected when β - $\text{NaYF}_4\text{:Ce@NaYF}_4\text{:Tb}$ core-shell nanoparticles were annealed in the solid state at temperatures higher than about 350 °C^[24], the β - $\text{NaYF}_4\text{:10\%Er@NaYbF}_4\text{@NaYF}_4$ nanoparticles were annealed at 400 °C for 4 h (ensuring detectable variation) to validate our assumption. Figure 5 shows the representative UCL spectra and decay curves of upconverted Er^{3+} emissions at 408, 541, and 654 nm for β - $\text{NaYF}_4\text{:10\%Er@NaYbF}_4\text{@NaYF}_4$ UCNPs under a 980-nm excitation before and after annealing. The intensity of the emissions at 408, 541, and 654 nm sharply decreased by 52%, 28%, and 4% [Figure 5A], and the corresponding lifetimes decreased from 0.62,

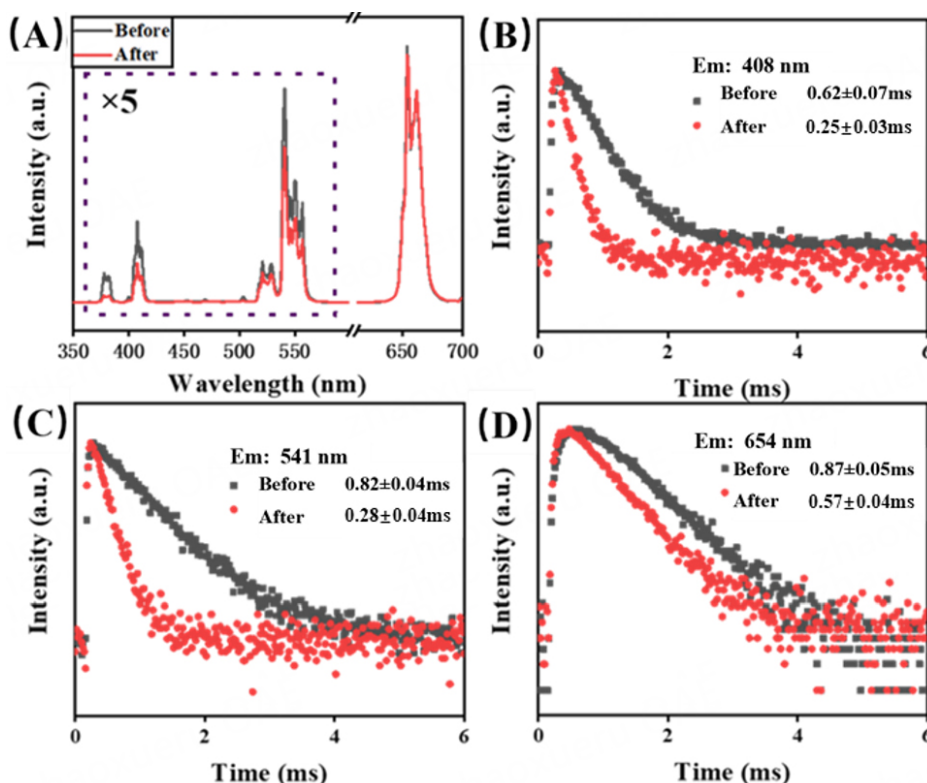


Figure 5. PL spectra (A) and decay curves of emissions at 407 (B); 540 (C); and 651 nm (D) for α - NaYF_4 :10%Er@ NaYbF_4 @ NaYF_4 UCNPs before and after annealing at 400 °C for 4 h (980-nm excitation).

0.82, and 0.87 ms to 0.25, 0.28, and 0.57 ms [Figure 5B–D], respectively. In addition to increased surface quenching, ion migration will also change Er/Yb concentrations in the core and the inner shell. In previous work, we have found that co-doping Yb at relatively lower concentration with Er in the core in this trilayered structure hardly affected red emission because increased Yb–Er cross-relaxation may benefit the red emission. In contrast, Yb–Er cross-relaxation led to fast decay of the blue emission^[26]. That is the possible reason why the intensity of red emission only decreases by 4% after annealing. Compared with α - NaYF_4 :10%Er@ NaYbF_4 @ NaYF_4 nanoparticles after annealing at 200 °C [Supplementary Figure 4], the descending rates of the upconversion emission from β -trilayered nanoparticles are much lower [Supplementary Figure 5], especially for the $^4\text{F}_{9/2} \rightarrow ^4\text{I}_{15/2}$ transition (654 nm). This dynamic may originate from the substantial fusion, aggregation, and growth of the crystalline grains, as revealed by the much narrower XRD peaks after annealing [Supplementary Figure 6A and B]. The TEM images [Supplementary Figure 6C and D] clearly confirm that the hexagonal NaYF_4 :10%Er@ NaYbF_4 @ NaYF_4 nanoparticles aggregated after annealing at 400 °C for 4 h. Partial grain fusion has also been observed by Chen *et al.* at 400 °C even though surface oleate ligands were removed in their work^[24]. The presence of residue oleate ligands [Supplementary Figure 2] herein might accelerate the grain growth since the local temperature may be higher than 400 °C due to the combustion of the oleate ligands. These results suggest that the diffusion and migration of Er^{3+} / Yb^{3+} / Y^{3+} across the core–intermediate shell and the intermediate shell–outmost shell interfaces lead to the descending UCL intensity and shorter decay times for β -phase nanoparticles even though the grain growth happens. In contrast to β -phase nanoparticles, apparent UCL degradation can be observed in α -phase counterparts after annealing at 200 °C, demonstrating lanthanide ions migration may be much easier in the latter lattice.

Simplified core-shell nanoparticles were adopted to provide direct experimental evidence for such heating-induced ion migration for these trilayered nanoparticles. In this regard, we synthesized α/β -NaErF₄@NaYF₄ core-shell UCNPs and compared their structural variation, especially surface elemental compositions, after heating at 200 °C for 4 h. As shown in Figure 6, despite the elongated shape, the as-synthesized α -NaErF₄@NaYF₄ core-shell nanoparticles have similar core sizes (around 10.5 nm), shell thicknesses (about 6.5 nm, approximately 12.5 nm for the longer axis) to those of β -NaErF₄@NaYF₄ UCNPs. The high-resolution TEM (HRTEM) images in the insets [Figure 6B and D] demonstrate the high crystallinity of these core-shell nanoparticles, consistent with the XRD patterns without any significant impurity phases [Supplementary Figure 7B and D]. After annealing at 200 °C for 4 h, the particle size, morphology, and crystalline phase of α/β -NaErF₄@NaYF₄ nanoparticles are essentially preserved [Supplementary Figure 7]. In accordance with the trilayered nanoparticles mentioned above, UCL intensity and lifetime of red emission at 665 nm descended significantly for α -NaErF₄@NaYF₄ nanoparticles, while the change in emission intensity and lifetime at 665 nm could be neglected for β -NaErF₄@NaYF₄ nanoparticles [Supplementary Figure 8].

In addition to the UCL intensity decrease, the corresponding quantum yields for the above nanoparticles also degraded after annealing [Supplementary Table 1], further demonstrating the possible heating-induced ion migration.

EDS mapping was used for observation of such possible ion migration. Despite the relatively lower resolution, it seems that the element Er diffused into the shell after annealing the α -NaErF₄@NaYF₄ nanoparticles [Supplementary Figure 9]. In contrast, the distribution of Er for β -NaErF₄@NaYF₄ nanoparticles remained nearly unchanged after annealing. In order to acquire strong evidence, XPS techniques were also adopted for detecting interfacial ion migration. If Er³⁺/Y³⁺ migrated across the core-shell interface, in addition to Y³⁺ ions, Er³⁺ ions could also appear in the shell. Consequently, interfacial ion migration could be simply detected by surface composition analyses. As shown in the XPS spectra [Figure 7A and C], only two peaks at approximately 159.0 and 161.1 eV can be detected at the surface of both as-prepared samples in the binding energy range of 155–175 eV, corresponding to 3d_{5/2} and 3d_{3/2} spectral lines of Y³⁺, respectively^[33]. These results demonstrate that the inert NaYF₄ shell is relatively thick, and no XPS signal from Er³⁺ in the core can be detected in this case. After annealing at 200 °C for 4 h, a new peak at about 166.2 eV, corresponding to Er 4d^[25,34], emerges, and Y 3d XPS peaks drop greatly for α -NaErF₄@NaYF₄ nanoparticles, while the XPS signals are unchanged for β -phase core-shell nanoparticles. Apparently, Er³⁺ ions in the core diffused into the shell part, and Y³⁺ ions in the shell diffused into the core during the annealing process in α -NaErF₄@NaYF₄ nanoparticles. As a result, the inert NaYF₄ shell became an active NaYF₄:Er shell, and thus the upconversion emission significantly declined since surface quenching is the major pathway of energy loss for erbium-enriched NaErF₄ nanoparticles^[35–39]. In contrast, no detected ion migration across the core-shell interface can be found in β -counterparts, consistent with their unchanged UCL intensity.

These results verify that the cation ions (Er³⁺/Y³⁺) in the α -phase nanoparticles are much easier to diffuse and migrate than those in the β -ones. This discrepancy may be related to their crystalline structures. The -NaREF₄ crystal has a high-symmetric fluorite structure similar to CaF₂, with the Ca²⁺ sites randomly occupied by Na⁺ and RE³⁺ [Figure 7B]. By contrast, there are three types of inequivalent cation sites in the β -NaREF₄ [Figure 7D] crystal, suggesting its higher order than α -NaREF₄. More importantly, the atoms are packed more loosely, and eight F⁻ ions form a large cubic void in the α -NaREF₄ lattice^[40]. This packing nature not only benefits interstitial F_i⁻ formation but also facilitates both cation and anion diffusion. Consequently, cation migration across the core-shell interface in α -NaREF₄ crystal needs relatively lower

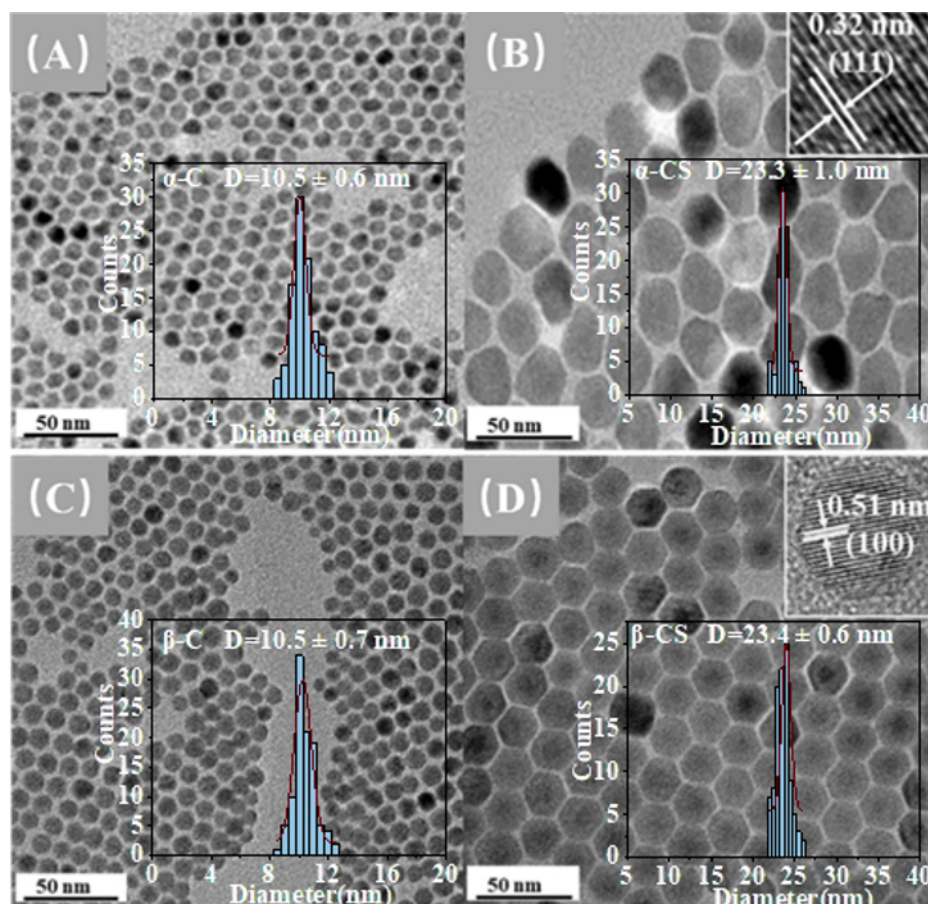


Figure 6. TEM images of α - (A-B) and β - (C-D) NaErF_4 core (A, C) and $\text{NaErF}_4\text{@NaYF}_4$ core-shell (B, D) nanoparticles. The size distribution histograms are shown in the insets. The size for elongated α - $\text{NaErF}_4\text{@NaYF}_4$ nanoparticles is represented by the shorter axes.

activation energy and occurs at a lower temperature than that in the β - NaREF_4 lattice. In this sense, both structural integrity change and thermal quenching should be considered for the application of β -phase core-shell nanoparticles as various luminescent probes even at a temperature no higher than 200 °C, especially for the condition in which the temperature change is not monotonic. In contrast, the structural integrity can be well maintained for β -phase core-shell nanoparticles ensuring more simple temperature-dependent UCL behavior in the same condition. Considering that the ion diffusion and migration can usually be accelerated in the solution, careful examination of the structural integrity of these α -phase core-shell nanoparticles is necessary before their practical usage in solution when stable upconversion emission is required.

CONCLUSIONS

Cubic and hexagonal $\text{NaYF}_4\text{:10%Er@NaYbF}_4\text{@NaYF}_4$ UCNPs were synthesized, and their temperature-dependent UCL was compared. In the temperature range of 298–498 K, an irreversible UCL variation was found in the former, while a reversible UCL change was observed in the latter. Unchanged crystalline phase and morphology after the two UCNP films were annealed at 200 °C, indicating their stable crystalline nature. At the same time, the change in surface compositions of cubic $\text{NaErF}_4\text{@NaYF}_4$ nanoparticles confirms that post-annealing resulted in $\text{Er}^{3+}/\text{Y}^{3+}$ migration across the core-shell interface. In contrast to cubic phase core-shell UCNPs, interfacial cation migration occurred at relatively higher temperatures for the hexagonal phase. We believe the loose packing atoms and the large cubic void consisting of eight F^- ions

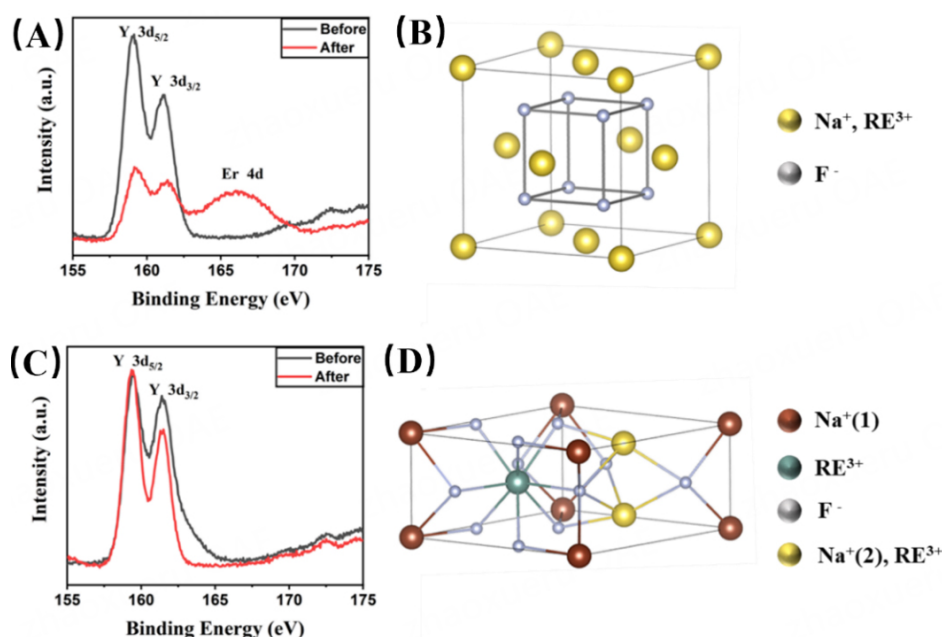


Figure 7. XPS spectra of α - (A) and β - (C) $\text{NaErF}_4\text{@NaYF}_4$ UCNPs before and after annealing at 200 °C for 4 h, crystalline structure of α - (B) and β - (D) NaREF_4 .

in the cubic phase core-shell UCNP benefit cations diffusion and migration, deteriorating their core-shell structural integrity and UCL properties. The densely packed hexagonal lattice may prohibit the interfacial cations diffusion, and the core-shell structure can be well maintained upon annealing at 200 °C. Our results suggest cation migration and structural invariability had better be considered if core-shell NaREF_4 UCNP are utilized in some practical applications.

DECLARATIONS

Acknowledgments

Here, the authors also want to thank the technical support from the Analytical and Testing Center at Huazhong University of Science and Technology.

Authors' contributions

Planned the study, analyzed the data, and prepared the manuscript: Qin CY, Ma Y
Performed manuscript correcting: Gao JH, Xie XB, Zhai CP

Availability of data and materials

The TG curve, XRD patterns, PL spectra, and TEM images of some samples are published as Supplementary Materials in the journal.

Financial support and sponsorship

This work was supported by the National Natural Science Foundation of China (No. 21871099) and the Fundamental Research Funds for the Central Universities.

Conflicts of interest

All authors declared that there are no conflicts of interest.

Ethical approval and consent to participate

Not applicable.

Consent for publication

Not applicable.

Copyright

© The Author(s) 2023.

REFERENCES

1. Liu Y, Lu Y, Yang X, et al. Amplified stimulated emission in upconversion nanoparticles for super-resolution nanoscopy. *Nature* 2017;543:229-33. DOI
2. Tan M, Li F, Wang X, Fan R, Chen G. Temporal multilevel luminescence anticounterfeiting through scattering media. *ACS Nano* 2020;14:6532-8. DOI
3. Nguyen NT, Huang K, Zeng H, et al. Nano-optogenetic engineering of CAR T cells for precision immunotherapy with enhanced safety. *Nat Nanotechnol* 2021;16:1424-34. DOI PubMed PMC
4. Fan Y, Wang P, Lu Y, et al. Lifetime-engineered NIR-II nanoparticles unlock multiplexed in vivo imaging. *Nat Nanotechnol* 2018;13:941-6. DOI
5. Rabie H, Zhang Y, Pasquale N, Lagos MJ, Batson PE, Lee KB. NIR biosensing of neurotransmitters in stem cell-derived neural interface using advanced core-shell upconversion nanoparticles. *Adv Mater* 2019;31:e1806991.
6. Zuo J, Tu L, Li Q, et al. Near infrared light sensitive ultraviolet-blue nanophotoswitch for imaging-guided "off-on" therapy. *ACS Nano* 2018;12:3217-25. DOI
7. Ren H, Huang F, Jiang J, Wang L, Zhang J. Development of photocatalyst based on NaYF₄: Yb, Tm@NaYF₄: Yb, Ce/NH₂-MIL-101 (Cr): Doping Ce³⁺ ions to promote the efficient energy transfer between core and shell. *Chem Eng J* 2022;427:132023. DOI
8. Huang F, Labrador-páez L, Ågren H, et al. Transient energy trapping as a size-conserving surface passivation strategy for producing bright ultrasmall upconversion nanoprobos. *Nano Energy* 2023;105:108015. DOI
9. Pan Y, Liu X, Zhang W, et al. Bifunctional template-mediated synthesis of porous ordered g-C₃N₄ decorated with potassium and cyano groups for effective photocatalytic H₂O₂ evolution from dual-electron O₂ reduction. *Chem Eng J* 2022;427:132032. DOI
10. Hao J, Zhang Y, Wei X. Electric-induced enhancement and modulation of upconversion photoluminescence in epitaxial BaTiO₃:Yb/Er thin films. *Angew Chem Int Ed Engl* 2011;50:6876-80. DOI
11. Yin W, Zhao L, Zhou L, et al. Enhanced red emission from GdF₃:Yb³⁺,Er³⁺ upconversion nanocrystals by Li⁺ doping and their application for bioimaging. *Chemistry* 2012;18:9239-45. DOI
12. Zhao J, Jin D, Scharfner EP, et al. Single-nanocrystal sensitivity achieved by enhanced upconversion luminescence. *Nat Nanotechnol* 2013;8:729-34. DOI
13. Wang J, Deng R, MacDonald MA, et al. Enhancing multiphoton upconversion through energy clustering at sublattice level. *Nat Mater* 2014;13:157-62. DOI
14. Zhou B, Yan L, Huang J, Liu X, Tao L, Zhang Q. NIR II-responsive photon upconversion through energy migration in an ytterbium sublattice. *Nat Photonics* 2020;14:760-6. DOI
15. Hofmann CLM, Fischer S, Eriksen EH, et al. Experimental validation of a modeling framework for upconversion enhancement in 1D-photonic crystals. *Nat Commun* 2021;12:104. DOI PubMed PMC
16. Huang F, Bagheri N, Wang L, et al. Low-lying excited state energy trap induced by cross-relaxation-The main origin of concentration quenching in lanthanide upconversion nanoparticles. *J Alloys Compd* 2023;936:168149. DOI
17. Zhong Y, Tian G, Gu Z, et al. Elimination of photon quenching by a transition layer to fabricate a quenching-shield sandwich structure for 800 nm excited upconversion luminescence of Nd³⁺-sensitized nanoparticles. *Adv Mater* 2014;26:2831-7. DOI
18. Chen X, Jin L, Kong W, et al. Confining energy migration in upconversion nanoparticles towards deep ultraviolet lasing. *Nat Commun* 2016;7:10304. DOI PubMed PMC
19. Liu Q, Zhang Y, Peng CS, Yang T, Joubert LM, Chu S. Single upconversion nanoparticle imaging at sub-10 W cm⁻² irradiance. *Nat Photonics* 2018;12:548-53. DOI PubMed PMC
20. Shi R, Brites CDS, Carlos LD. Understanding the shell passivation in Ln³⁺-doped luminescent nanocrystals. *Small Structures* 2022;3:2100194. DOI
21. Dühnen S, Haase M. Study on the intermixing of core and shell in NaEuF₄/NaGdF₄ core/shell nanocrystals. *Chem Mater* 2015;27:8375-86. DOI
22. Hudry D, Popescu R, Busko D, et al. Interface disorder in large single- and multi-shell upconverting nanocrystals. *J Mater Chem C* 2019;7:1164-72. DOI
23. Bastian PU, Nacak S, Roddatis V, Kumke MU. Tracking the motion of lanthanide ions within core-shell-shell NaYF₄ nanocrystals via resonance energy transfer. *J Phys Chem C* 2020;124:11229-38. DOI
24. Chen B, Peng D, Chen X, Qiao X, Fan X, Wang F. Establishing the structural integrity of core-shell nanoparticles against elemental

- migration using luminescent lanthanide probes. *Angew Chem Int Ed Engl* 2015;54:12788-90. DOI
25. Liu L, Li X, Fan Y, et al. Elemental migration in core/shell structured lanthanide doped nanoparticles. *Chem Mater* 2019;31:5608-15. DOI
 26. Zhou B, Tang B, Zhang C, et al. Enhancing multiphoton upconversion through interfacial energy transfer in multilayered nanoparticles. *Nat Commun* 2020;11:1174. DOI PubMed PMC
 27. Roberts JE. Lanthanum and neodymium salts of trifluoroacetic acid. *J Am Chem Soc* 1961;83:1087-8. DOI
 28. Zhou B, Xu B, He H, et al. Enhanced green upconversion luminescence in tetrahedral LiYF₄:Yb/Er nanoparticles by manganese(ii)-doping: the key role of the host lattice. *Nanoscale* 2018;10:2834-40. DOI
 29. Wang F, Deng R, Liu X. Preparation of core-shell NaGdF₄ nanoparticles doped with luminescent lanthanide ions to be used as upconversion-based probes. *Nat Protoc* 2014;9:1634-44. DOI PubMed
 30. Zhou Y, Cheng Y, Xu J, Lin H, Wang Y. Thermo-enhanced upconversion luminescence in inert-core/active-shell UCNPs: the inert core matters. *Nanoscale* 2021;13:6569-76. DOI
 31. Wu X, Zhan S, Han J, Liu Y. Nanoscale ultrasensitive temperature sensing based on upconversion nanoparticles with lattice self-adaptation. *Nano Lett* 2021;21:272-8. DOI PubMed
 32. Wang Y, Zhou S, Hu P, Zhong W, Fu J. Temperature-sensitive lanthanide-doped core-multishell nanocrystals with excitation-wavelength-dependent bimodal luminescence thermo-behaviors and their application in dynamic anticounterfeiting. *J Alloys Compd* 2023;938:168442. DOI
 33. Uwamino Y, Tsuge A, Ishizuka T, Yamatera H. X-Ray photoelectron spectroscopy of rare earth halides. *BCSJ* 1986;59:2263-7. DOI
 34. Powell C. Elemental binding energies for X-ray photoelectron spectroscopy. *Appl Surf Sci* 1995;89:141-9. DOI
 35. Huang J, Li J, Zhang X, et al. Artificial Atomic vacancies tailor near-infrared II excited multiplexing upconversion in core-shell lanthanide nanoparticles. *Nano Lett* 2020;20:5236-42. DOI
 36. Johnson NJ, He S, Diao S, Chan EM, Dai H, Almutairi A. Direct evidence for coupled surface and concentration quenching dynamics in lanthanide-doped nanocrystals. *J Am Chem Soc* 2017;139:3275-82. DOI PubMed
 37. Chen Q, Xie X, Huang B, et al. Confining excitation energy in Er³⁺-sensitized upconversion nanocrystals through Tm³⁺-mediated transient energy trapping. *Angew Chem Int Ed Engl* 2017;56:7605-9. DOI
 38. Wang Y, Zhou S, Sun F, Hu P, Zhong W, Fu J. In-depth insight into the Yb³⁺ effect in NaErF₄-based host sensitization upconversion: a double-edged sword. *Nanoscale* 2022;14:16156-69. DOI
 39. Zhou S, Wang Y, Hu P, et al. Cascaded photon confinement-mediated orthogonal RGB-switchable naerf₄-cored upconversion nanoarchitectures for logicalized information encryption and multimodal luminescent anti-counterfeiting. *Laser Photonics Rev* 2023;17:2200531. DOI
 40. Wang F, Han Y, Lim CS, et al. Simultaneous phase and size control of upconversion nanocrystals through lanthanide doping. *Nature* 2010;463:1061-5. DOI